Modeling the Vapor Pressure of Biodiesel Fuels

O. Castellanos Díaz, F. Schoeggl, H. W. Yarranton, M. A. Satyro, T. M. Lovestead, and T. J. Bruno

Abstract—The composition, vapour pressure, and heat capacity of nine biodiesel fuels from different sources were measured. The vapour pressure of the biodiesel fuels is modeled assuming an ideal liquid phase of the fatty acid methyl esters constituting the fuel. New methodologies to calculate the vapour pressure and ideal gas and liquid heat capacities of the biodiesel fuel constituents are proposed. Two alternative optimization scenarios are evaluated: 1) vapour pressure only; 2) vapour pressure constrained with liquid heat capacity. Without physical constraints, significant errors in liquid heat capacity predictions were found whereas the constrained correlation accurately fit both vapour pressure and liquid heat capacity.

Keywords—Biodiesel fuels, Fatty acid methyl ester, Heat capacity, Modeling, Vapour pressure

I. INTRODUCTION

A biodiesel fuel is the refined mixture of esters produced by the transesterification of fatty acids from vegetable oil and animal fat (fatty acid methyl esters or FAMEs for short) [1, 2, 3]. These mixtures constitute one of the most promising alternatives for the partial replacement of petroleum-based diesel fuel (petro-diesel). They are renewable, non-mutagenic, non-carcinogenic, biodegradable fuels that can be domestically produced [3, 4]. Biodiesel fuels can be used directly or blended with petroleum diesel, especially low-sulphur fuels, to improve their lubricity without adding any sulphur. These fuels may also improve engine firing because they consist of oxygenated molecules [4]. In order to deploy biodiesel fuels commercially, it is necessary to measure or predict their properties. One important property for the quality control of biodiesel fuels and their blends is volatility, which is directly related to their constituent vapour pressures [2]. For instance, vapour pressure is used to calculate the heat of vaporization in order to compare rates of vaporization and injection characteristics with other fuels. Vapour pressures are also used to assess the cold weather properties of these fuels. Yuan et al. [5] modeled the vapour pressure of three different biodiesel fuels at temperatures above 215 °C using Raoult's law and the constituent FAME vapour pressures [1, 2]. However, experimental physical properties data for fatty acids and fatty acids methyl esters and biodiesel fuels are scarce and need further development, particularly at lower temperatures.

This paper introduces an improved vapour pressure model applicable for moderate temperatures using an optimization strategy constrained by heat capacity and vapour pressure data. New correlations for FAME heat capacity and vapour pressure are also presented.

II. EXPERIMENTAL

Compositional, liquid heat capacity, and vapour pressure data for the biodiesel fuels are required to validate the proposed modeling methodology. Table I shows a list of the biodiesel fuels assessed in this research for this purpose, as well as the temperature range of the vapour pressure and heat capacity experimental data. The composition, vapour pressure, and liquid heat capacity of the first nine biodiesel fuels were measured as part of this work. The vapour pressures of the last three biodiesel fuels were obtained from the open literature.

A. Biodiesel Fuels Composition

The components of each of the biodiesel fuels samples were identified with gas chromatography and mass spectrometry (GC-MS). First, the sample was injected with an automatic sampler into a split/splitless injector set to a 100:1 split ratio. The injector was maintained at a temperature of 350 °C and operated at a constant head pressure of 173 kPa. The stationary phase was a 0.1 µm coating of 50 % cyanopropyl-50 % dimethyl polysiloxane, with a temperature program (80 °C for 2 min, 8 °C per min to 220 °C, followed by a 220 °C hold for 5 min). This stationary phase provides separations based upon polarity and is specifically intended for the analysis of the FAME compounds that make up biodiesel fuels, and the temperature program is typical for the analysis of such mixtures. Mass spectra were collected and interpreted for each peak from 33 to 750 relative molecular mass (RMM) units [6, 7, 8, 9].

Once the components were identified, the biodiesel fuel samples were analyzed with gas chromatography and flame ionization detection (GC-FID) with external standards to determine mass fraction of each component. FAMEs ranging from C6:0 to C20:1 were identified; with the exception of sample S070717, the majority of each fuel was composed of C18:0, C18:1, and C18:2. Table II summarizes the composition results for the biodiesel fuels listed in Table I. The uncertainty of this data set is approximately 2 %.

O.C.D., F.S., and H.W.Y are with the Department of Chemical and Petroleum Engineering, University of Calgary, AB, Canada (e-mail: hyarrant@ucalgary.ca).

M.A.S is with Virtual Materials Group, Calgary, AB, Canada (e-mail: marco.satyro@virtualmaterials.com).

T.M.L and T.J.B are with the National Institute of Standards and Technology, Boulder, CO, United States (e-mail: bruno@boulder.nist.gov).

TABLE I
TEMPERATURE RANGE OF VAPOR PRESSURE AND HEAT CAPACITY DATA FOR SELECTED BIODIESEL FUELS

Biodiesel fuels Source	Code	Vapour Pressure	Liquid Heat Capacity	Reference
Canola (South Alberta)	CB-01	60-196 °C	13-55 °C	This work
Canola (Saskatchewan)	I-25	-	12-55 °C	This work
Soy (Sunrise, US)	SB100	-	14-55 °C	This work
Soy (Mountain Gold, US)	MGB100	140 °C	10-55 °C	This work
Rapeseed (Europe)	S102550	80-110 °C	13-55 °C	This work
Palm (Europe)	S090824	70-100 °C	23-55 °C	This work
Coconut (Europe)	S070717	95-125 °C	10-55 °C	This work
Tallow (Alberta)	I26	-	8-55 °C	This work
Tallow (South Alberta)	Sylfat	-	25-55 °C	This work
Soybean (Idaho)		275-350 °C	-	[2]
Rapeseed (Idaho)		215-360 °C	-	[2]
Beef Tallow (Idaho)		255-340 °C	-	[2]

Certain commercial equipment, materials or supplies are identified in this paper to adequately specify the experimental procedure or description. Such identification does not imply recommendation or endorsement by the National Institute of Standards and Technology, nor does it imply that the equipment, materials or supplies are the best available for the purpose.

B. Biodiesel Fuel Liquid Heat Capacity

The liquid heat capacity of the biodiesel fuel samples was measured using a differential scanning calorimeter (DSC) TA Q2000 V24.9 calibrated against indium. The samples were heated at a rate of 5 °C/min from -40 °C to 60 °C and the amount of heat input was recorded. By comparison of the heat flow, the temperature ramp, and the calibration standard, the heat capacity curve of the sample was determined as a function of temperature [10, 11]. The liquid heat capacity is reported at temperatures 2-10 °C above the cloud point to 55 °C, Table I.

C. Biodiesel Fuel Vapor Pressure

The vapour pressure of biodiesel fuels was measured using a new static apparatus, Figure 1. The apparatus is designed to perform a series of P-X flashes on a given sample, similar to a differential liberation test. To perform an experiment, the sample vessel is isolated and the rest of the apparatus is placed under a vacuum (the base line pressure) at a pressure below the expected vapour pressure. Then, the sample is opened to the vacuum and the pressure is monitored. Finally, the sample is again isolated and the apparatus is brought back to the base line vacuum. This single flash measurement cycle is repeated as required. An example of the pressure reading for a number of cycles is provided in Figure 2.

Samples to be measured may contain lighter impurities. In particular, biodiesel fuels are prone to absorb moisture from the surrounding air [12]. Also, air is always trapped inside the walls of the apparatus when it is exposed to the atmosphere. These impurities may adversely affect the accuracy of the vapour pressure measurement. In order to remove the impurities, several measurement cycles are run as shown in Figure 2. The plot can be divided in three sections: 1) high pressure peaks that are attributed to trapped air; 2) more uniform but decreasing pressure peaks that are attributed to the water and some solvents in the sample; 3) uniform pressure peaks attributed to the vapour pressure of the sample.

Sections 1 and 2 are known as the degassing section whereas Section 3 is the measurement section.
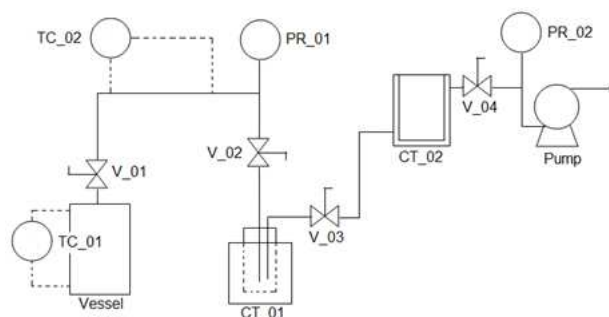

Fig. 1 chematics of static vapour pressure measurement apparatus; V_01, 02, 03, 04: rubber-sealed in-line valves; TC_01, 02: temperature controllers; PR_01, 02: pressure readers; CT_01, 02: cold traps; vessel: 1/2" inch metal full nipple; pump: turbo-molecular pump
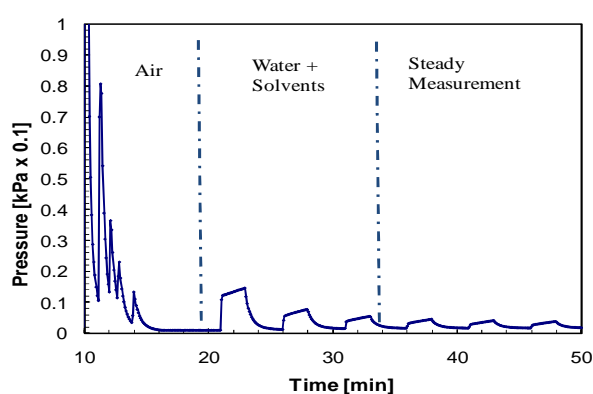

Fig. 2 Degassing and vapour pressure measurement cycles using apparatus in Figure 1

TABLE II
COMPOSITION IN MOLE PERCENTAGE OF FAMEs IN SELECTED BIODIESEL FUELS

FAMEs	CB-01	I-25	SB100	MGB100	S102550	S090824	S070717	I26	Sylfat
C6:0	0	0	0	0	0	0	1.0	0	0
C8:0	0	0	0	0	0	0	12.6	0	0
C10:0	0	0	0	0	0	0	7.7	0	0
C12:0	0	0	0	0	0	0	48.3	0	0
C14:0	0	0	0	0.6	0	1.5	16.6	3.4	0
C15:0	0	0	0	0	0	0	0	0.6	0
C16:1	12.7	0.9	0	0.5	0	0	0	2.9	0
C16:0	12.7	9.3	11.4	12.5	4.8	45.1	6.7	25.6	10.0
C17:0	0	0.3	0	0	0	0	0	1.2	20.2
C17:1	0	0	0	0	0	0	0	0	7.9
C17:1	0	0	0	0	0	0	0	0	7.9
C18:0	4.1	4.4	3.2	4.9	1.28	3.6	1.5	14.8	25.3
C18:1(9)	23.5	57.4	21.3	27.0	59.91	39.5	4.4	42.8	26.5
C18:1(11)	1.5	2.8	1.5	1.6	3.68	0	0	1.6	2.3
C18:2	49.9	16.0	54.9	46.6	19.44	9.8	1.1	5.8	3.6
C18:3	8.1	7.5	7.4	6.1	9.08	0.2	0	1.1	4.2
C20:0	0.2	0.4	0.3	0.3	1.26	0.3	0	0.2	0
C20:1	0	1.00	0	0	0.55	0	0	0	0
MW$_{avg}$	291.5	293.2	291.8	291.3	294.6	283.7	218.2	286.8	301.3

III. VAPOR PRESSURE MODELING

The vapour pressure of the biodiesel fuels is calculated assuming an ideal solution of the constituent FAMEs (Raoult's law).

$$P_{Biodiesel}^{Calc} = \sum_j x_j P_j \tag{1}$$

where x and P are the mole fraction and total ideal vapour pressure of component j, respectively.

A correlation is required to determine the vapour pressure of the FAMEs. Růžička and Majer [13] recommend the Cox equation, among the common vapour pressure equations, to be used when extrapolation is required. This equation has the advantage of not depending on critical properties. In this work, a three degree Cox equation was used [13]:

$$\ln\left(\frac{P_V}{P_{Ref}}\right) = \left(1 + \frac{T_{Ref}}{T}\right) \exp\left(a_{Pv,0} + a_{Pv,1}T + a_{Pv,2}T^2\right) \tag{2}$$

where P_{Ref} is a reference pressure at T_{Ref}, and $a_{PV,1-2-3}$ are the correlation constants. The reference state in the Cox equation should be one close to where the extrapolation is intended. In this case, it is convenient to choose the normal melting point (NMP) of the FAMEs as a reference state. NMP values were obtained from the NIST data base [14]. Note that the vapour pressure of the FAMEs at their NMP is typically unknown and is treated as a fourth adjustable parameter in Equation 2.

For substances with high molecular weights such as biodiesel fuels (MW~250 g/mol), it is a challenge to obtain accurate vapour pressure data with which to determine the parameters for the Cox equation. The vapour pressure of these components can be lower than 10^{-4} kPa at low to moderate temperatures. At these pressure values, the accuracy of direct pressure readings decreases dramatically due to adsorption-desorption and permeation processes inside the measurement apparatus [15, 16].

To overcome this issue, indirect measurements such as effusion or transpiration (i.e. gas chromatography) methods are performed [11]. However, these techniques may generate new sources of error coming from the experimental method and/or the processing of the data.

An alternative to indirect measurements is to extrapolate accurate vapour pressure data points measured above 10^{-4} kPa towards lower values. It is advisable to constrain the vapour pressure equation using calorimetric data since these two physical properties are directly related via the Clausius-Clapeyron equation and the definition of heat capacity at constant pressure, $C_P = dH/dT$:

$$\Delta C_{P,j} = R\left[\frac{d}{dT}T^2\left(\frac{d \ln P_j}{dT}\right)\right] \tag{3}$$

The vapour pressure correlation can then be constrained as follows [13]:

$$\min j = \sum_i \left(\ln P_i^{Exp} - \ln P_i^{Calc}\right)^2 + K_C \sum_i \left(\Delta C_{P,i}^{Exp} - \Delta C_{P,i}^{Calc}\right)^2 \tag{4}$$

where j is the objective function to be minimized, P represents the pressure of the biodiesel fuel, ΔC_P is the phase transition heat capacity difference between liquid and vapour phases, K_C is a weight factor and i stands for the experimental data points. For an ideal solution assumption, the phase transition heat capacity is given by:

$$\Delta C_{P,biodiesel}^{Calc} = \sum_j x_j \Delta C_{P,j} \tag{5}$$

To use this method for biodiesel fuels, FAME vapor pressures are required (in this work, experimentally obtained at higher temperatures and extrapolated to lower temperatures) and FAME heat capacities are required that extend to the lower temperatures of interest.

IV. FAMES PROPERTIES

Eighteen FAMEs ranging in carbon number from 6 to 22 were assessed, as presented in Table III. The vapour pressure data set ranges in temperature from 25 to 300 ºC whereas liquid heat capacity data range from the freezing point to 50

ºC. Since data were not available for all FAMEs, the modeling approach was developed in four steps: 1) develop a correlation to estimate the phase transition heat capacities; 2) fit the constrained vapour pressure equation to the available vapour pressure data; 3) develop a vapour pressure correlation for FAMEs for which data are not available; 4) predict the vapour pressure of the FAMEs with unavailable data.

A. Heat Capacity

The phase transition heat capacity is determined as follows:

$$\Delta C_{P,FAME} = C_{P,L,FAME} - C_{P,V,FAME} \approx C_{P,L,FAME} - C_{P,FAME}^0 \quad (6)$$

where C_{PL}, C_{PV}, and C_P^0 stand for the liquid, vapour, and ideal gas heat capacity. Note that since we are concerned with low vapour pressures, the vapour phase can be regarded as ideal and $C_{P,V} \approx C_P^0$ [13]. Hence, correlations for the ideal gas and liquid heat capacity are required.

1) Ideal Gas Heat Capacity

First, the ideal gas heat capacity of the saturated FAMEs with available liquid heat capacity data (Table I) was calculated as follows:

$$C_{P,FAME}^0 = C_{P,L,FAME} - C_{P,FAME}^{Residual} \quad (7)$$

where $C_P^{Residual}$ is the residual or departure function of the heat capacity and is calculated using the Peng-Robinson equation of state [17]. Then, the ideal gas heat capacity of these FAMEs was regressed with a second degree polynomial

$$C_P^0(0) = a_{Cp0} + b_{Cp0}T + c_{Cp0}T^2 \quad (8)$$

Figure 3 shows the calculated and regressed ideal gas heat capacity values for methyl caprylate, C10:0
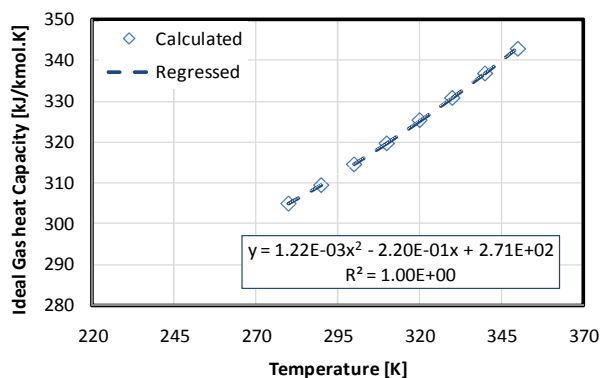

Fig. 3 Calculated and regressed ideal gas heat capacity for methyl caprylate, C10:0

To generalize Equation 8 for all saturated FAMEs, its parameters were plotted as a function of the molecular mass, Figure 4, and fitted as follows

$$a_{CP0} = \frac{-2.108\,x10^4}{MW - 344.176} + 230.72$$
$$+ 0.625(MW - 344.176) \quad (9)$$

$$b_{CP0} = \frac{125.93}{MW - 344.176} + 1.453$$
$$+ 5.555\,x10^{-3}(MW - 344.176) \quad (10)$$

$$c_{CP0} = \frac{-0.1913}{MW - 344.176} - 8.863\,x10^{-4}$$
$$- 5.999\,x10^{-6}(MW - 344.176) \quad (11)$$

No data were available for the ideal gas heat capacity of the unsaturated FAMEs. Hence, it is assumed that the departure function from the corresponding saturated FAME is equal to the same departure function as calculated by Joback's method [17]. The departure function from Joback's method is given by:

$$\frac{C_P^0(N_{UC})}{C_P^0(0)} = \frac{N_{CH_3}\sum_{i=0}^{3} a_i T^i + N_{CH_2}\sum_{i=0}^{3} b_i T^i + N_{COO}\sum_{i=0}^{3} c_i T^i + N_{UC}\sum_{i=0}^{3} d_i T^i + \sum_{i=0}^{3} e_i T^i}{N_{CH_3}\sum_{i=0}^{3} a_i T^i + N_{CH_2}\sum_{i=0}^{3} b_i T^i + N_{COO}\sum_{i=0}^{3} c_i T^i + \sum_{i=0}^{3} e_i T^i} \quad (12)$$

where N_{UC} is the number of unsaturated bonds (1, 2, or 3), N_{CH3}, N_{CH2}, and N_{COO} are the number of function groups within the molecule, and a, b, c, d, and e are standard parameters for the method. Equation 12 simplifies to the following expression

$$\frac{C_P^0(N_{UC})}{C_P^0(0)} = \left[1 + N_{UC}\left(\begin{array}{c}-6.1327\,x10^{-2}\\+1.5493\,x10^{-4}T - 1.842\,x10^{-7}T^2\end{array}\right)\right] \quad (13)$$

2) Liquid Heat Capacity

Initially, the Dadgostar-Shaw [18] equation was used to calculate the liquid heat capacity of the FAMEs as follows:

$$c_{PL} = a_1(\alpha) + a_2(\alpha)T + a_3(\alpha)T^2 \quad (14)$$

where T is the temperature in Kelvin and α is a similarity variable which is related to the elementary composition of a substance as follows:

$$\alpha = \frac{\sum_k v_k}{\sum_k v_k MW_k} \quad (15)$$

The different functions of α are given by:

$$a_1(\alpha) = 24.5(-0.3416\alpha + 2.2671\alpha^2) \quad (16)$$

TABLE III
DATA AVAILABLE FOR SELECTED FAMES AND TEMPERATURE RANGE IN °C [14]

FAME	Formula	P_V			C_{PL}		
		Points	T_{min}	T_{max}	Points	T_{min}	T_{max}
Methyl hexanoate	C6:0	65	7.55	146.52	-	-	-
Methyl caprylate	C8:0	53	33.69	145.70	12	-33.15	76.85
Methyl caprate	C10:0	70	-12.74	188.20	10	-3.15	76.85
Methyl laurate	C12:0	112	-11.00	226.85	8	6.85	76.85
Methyl myristate	C14:0	90	0.00	237.8	7	25	76.85
Methyl pentadecanoate	C15:0	29	21.85	226.85	5	26.85	76.85
Methyl palmitate	C16:0	110	18.00	321.95	5	36.85	76.85
Methyl heptadecanoate	C17:0	27	21.85	226.85	5	36.85	76.85
Methyl stearate	C18:0	101	21.85	346.95	4	46.85	76.85
Methyl arachidate	C20:0	29	38.00	226.85	3	56.85	76.85
Methyl behenate	C22:0	12	21.85	258.95	-	-	-
Methyl lignocerate	C24:0	-	-	-	-	-	-
Methyl palmitoleate	C16:1	4	26.85	176.85	-	-	-
Methyl heptadecenoate	C17:1	-	-	-	-	-	-
Methyl oleate	C18:1(11)	33	26.85	218.50	-	-	-
Methyl vaccenate	C18:1(9)	-	-	-	-	-	-
Methyl cis-11-eicosenoate	C20:1(11)	-	-	-	-	-	-
Methyl erucate	C22:1	8	26.85	176.85	-	-	-
Methyl linoleate	C18:2	18	26.85	214.95	-	-	-
Methyl linolenate	C18:3	12	26.85	185.7	-	-	-

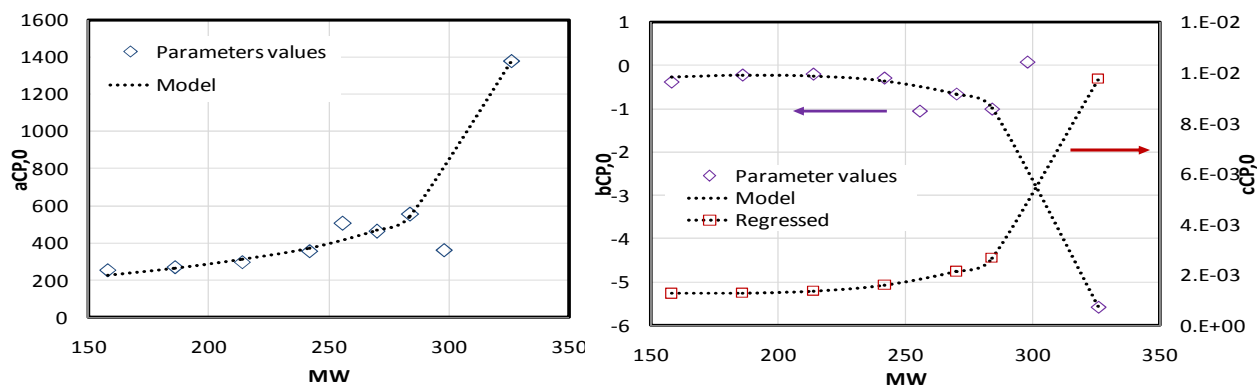
Fig. 4 Mapping nonlinear data to a higher dimensional feature space

$$a_2(\alpha) = -0.1064 \pm 0.3874\alpha^2 \qquad (17)$$
$$a_3(\alpha) = -9.8231x10^{-5} + 4.182x10^{-4}\alpha^2 \qquad (18)$$

Equation 14 was applied to calculate the available liquid heat capacity experimental data of the FAMEs listed in Table 1, with an absolute average relative deviation (AARD) of 2.4%. To improve this accuracy, a modification of Equation 14 is proposed:

$$C_{PL} = (2.279 + a_1(\alpha)) + (-6.956\,x10^{-3} + a_2(\alpha))T + (9.509\,x10^{-6} + a_3(\alpha))T^{21} \qquad (19)$$

Figure 5 shows experimental and predicted liquid heat capacity data of methyl palmitate. The FAME specific modification improves the accuracy with an AARD of all of the assessed FAMEs of 0.72%.
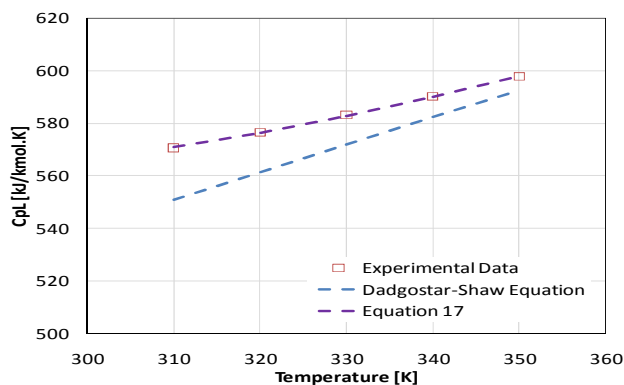
Fig. 5 Experimental and predicted liquid heat capacity for C16:0.
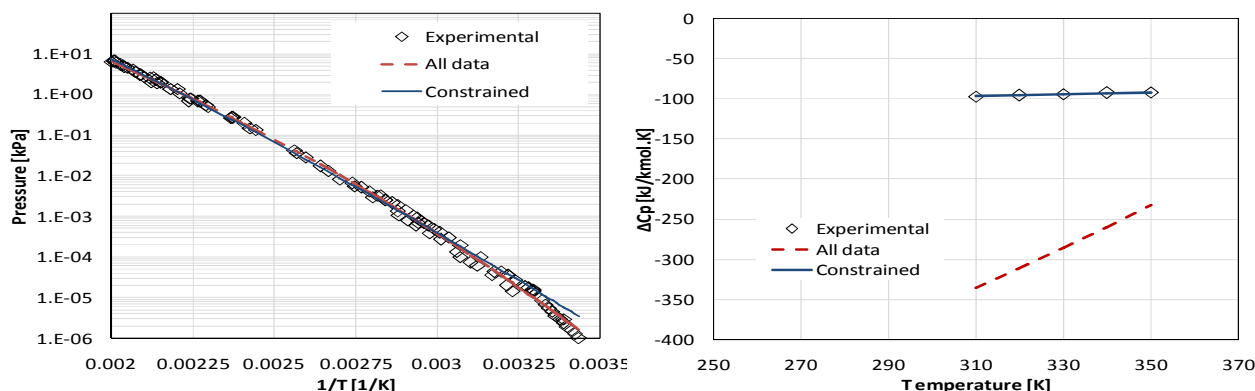Data from NIST [14]

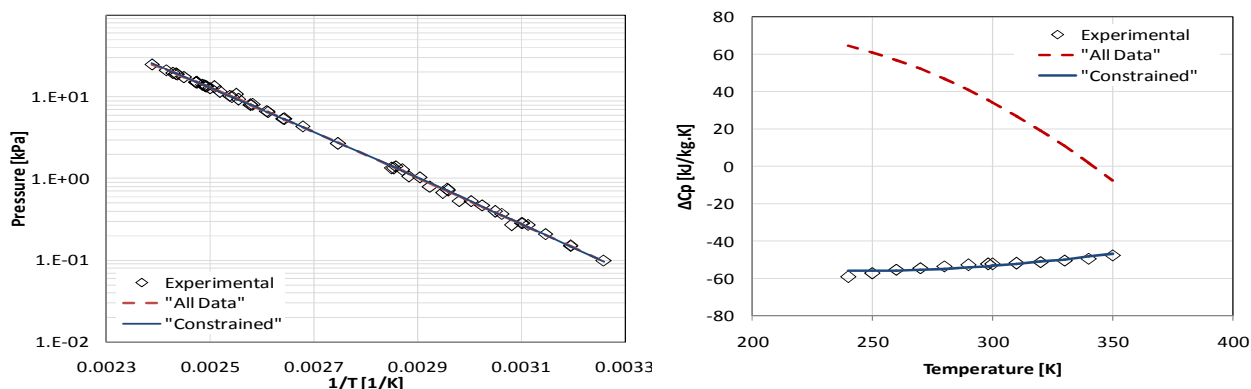Fig. 6 Experimental and regressed vapor pressure of methyl palmitate (Data from NIST [14])

Fig. 7 Experimental and regressed vapor pressure of methyl caprylate (Data from NIST [14])

B. Vapor Pressure Fitting

The Cox equation (Equation 2) was adjusted to the vapour pressure of the FAMEs using the constrained optimization (Equation 4). Two scenarios were evaluated: Scenario 1: "All-data" is a regression of all the vapour pressure data available with no constraints ($K_C = 0$ in Equation 4); Scenario 2: "Constrained" is a regression of vapour pressure data above 10^{-4} kPa constrained with liquid heat capacity (a value of $K_C = 1/100$ in Equation 4 scales the heat capacity data in kJ/kmol.K to the same magnitude as the natural log of the vapour pressure data in kPa). Table IV shows the regressed coefficients for both scenarios.

Figure 6 shows the results for methyl palmitate. Note that the majority of experimental values below 10^{-4} kPa were indirect, most of them coming from gas chromatography experiments [14]. Figure 6 shows that both regression scenarios fit the vapour pressures above 10^{-4} kPa but the constrained fit departs from the data at lower pressures (higher deviations were found with heavier FAMEs). However, the liquid heat capacity values calculated with unconstrained vapour pressure data always deviated from literature data. In addition, in some cases, the heat capacity predicted with the unconstrained equation incorrectly decreased with temperature, as shown in Figure 7 for methyl caprylate.

The constrained regression produced consistent, accurate predictions of the heat capacity. The AARD values for vapour pressure and heat capacity for all of the FAMEs are 6.7% and 158% in the "All-data" scenario, and 9.0% and 0.7%for the "Constrained" scenario, respectively. Since heat capacity and vapour pressure are related, the "Constrained" correlation is expected to provide a more accurate prediction of the low vapour pressures than the "all data" correlation.

C. Vapor Pressure Prediction

A new methodology to predict vapour pressure for FAMEs is introduced. For convenience, it is divided into saturated and unsaturated FAMEs vapour pressure.

1) Saturated FAMEs Vapor Pressure Equation

In developing the new vapour pressure correlation for saturated FAMEs, the data listed in Table 3 was used as a training set and experimental data of methyl nonadecanoate (C19:0) was used to test the correlation. At a given temperature, 70 ºC in Figure 8, the vapour pressure changes exponentially with the carbon number, as follows:
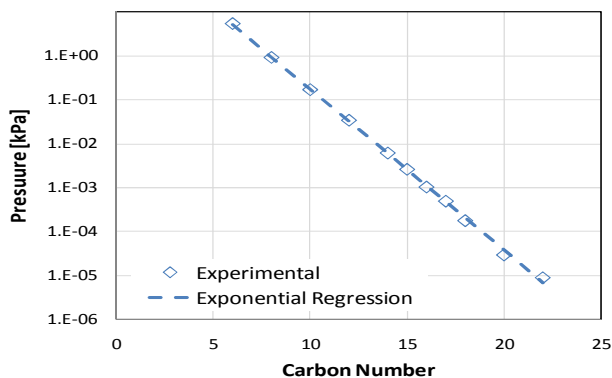
Fig. 8 Mapping nonlinear data to a higher dimensional feature space

$$P(N_C)|_T = a_{CN,0} \exp[a_{CN,1} N_C] \qquad (20)$$

where N_C is the carbon number from the fatty acid formula N_C:0, and $a_{CN,i}$ are correlation parameters. Each parameter is plotted as a function of the temperature, Figure 9, and fitted as follows:

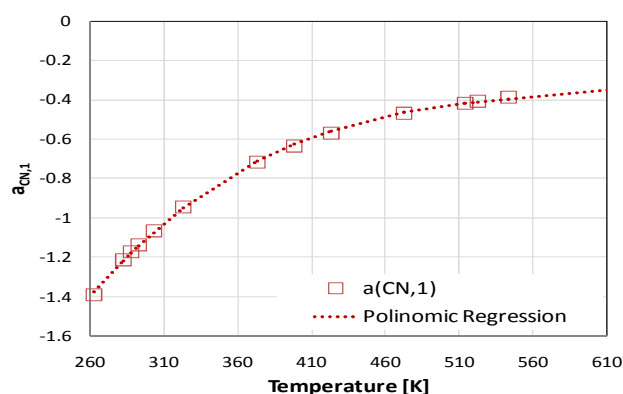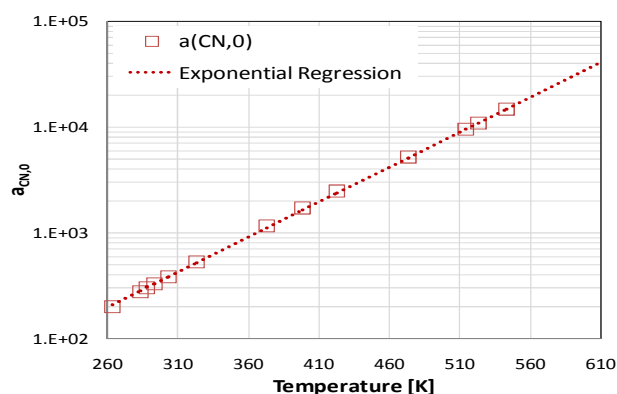$$a_{CN,0} = 1.908 \exp[0.01715\,T] \qquad (21)$$

Figure 10 (left) shows the experimental data and predictions for the training set. To test Equations 19 to 21, the vapour pressure of C19:0 was predicted, Figure 10 (right). The model predicts the vapour pressure with an AARD of 2.8%.

2) Unsaturated FAMEs Vapor Pressure Equation

For unsaturated FAMEs the amount of experimental data is very small which, in turn, limits the scope of any method based on this data. Data for C18:0, C18:1, C18:2 and C18:3 were used to develop a preliminary correlation; data for C16:1 was used to corroborate the method. Figure 11 shows the experimental data and correlation results for the training set.

At high temperatures, any differences among the vapour pressure of the different FAMEs are virtually undistinguishable from the experimental error. However, at low temperatures, the differences become apparent. Therefore, the following departure function is proposed for the unsaturated FAMEs at temperatures below 50 °C (323 K)

$$a_{CN,1} = -5.656 + 0.02649\,T \qquad (22)$$
$$- 4.5417\,x10^{-5}\,T^2 + 2.6571\,x10^{-8}\,T^3$$
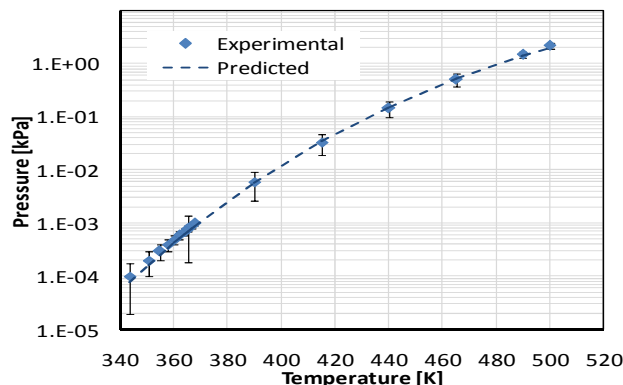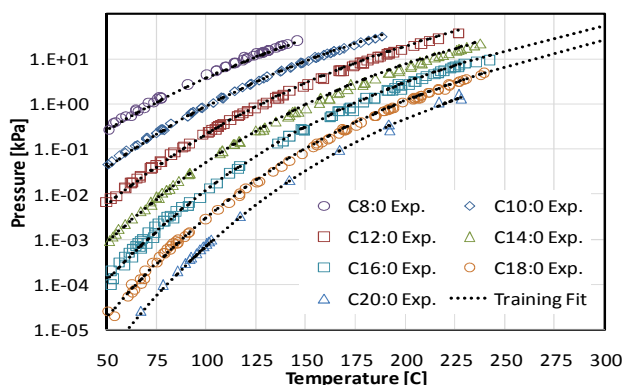

Fig. 9 $a_{CN,0}$ and $a_{CN,1}$ parameters in Equation 18 as a function of temperature

Fig. 10 Experimental and predicted values for the training set (left) and the tester, methyl nonadecanoate (right)
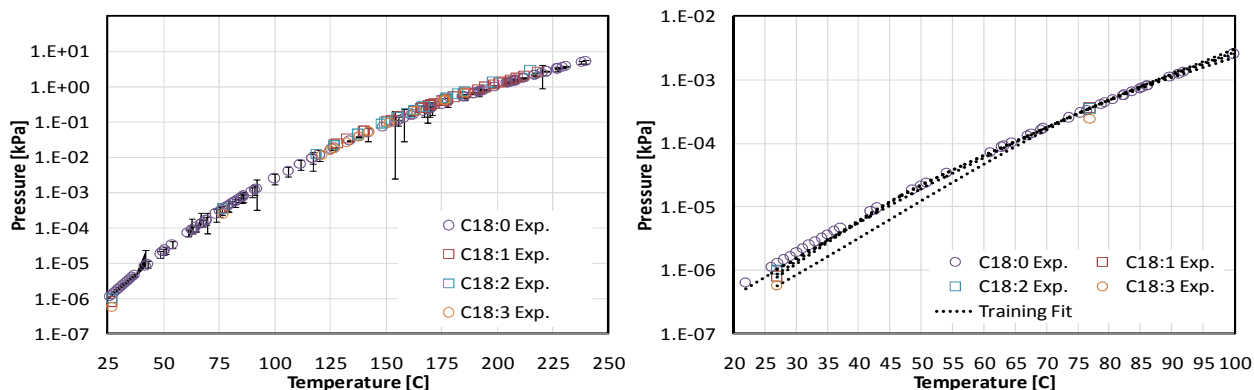
Fig. 11 Experimental and correlated vapour pressure datafor unsaturated C18 family of FAMEs at 30 °C

$$\frac{P_V(N_{UC})_T}{P_V(0)_T} = a_{UC}(N_{UC} + 1) + b_{UC} + \frac{c_{UC}}{N_{UC}+1} \qquad (23)$$

where N_{UC} is the number of unsaturated double bonds and a_{UC}, b_{UC}, and c_{UC} are the correlation parameters which are related to temperature as follows:

$$a_{UC} = 4.62\,x10^{-5}\,T^2 - 3.06\,x10^{-2}\,T + 5.05$$
$$T \leq 323\,K \qquad (24)$$
$$a_{UC} = 0$$
$$T > 3.23\,K$$
$$b_{UC} = 3.39\,x10^{-2}\,T - 9.93$$
$$T \leq 323\,K \qquad (25)$$
$$b_{UC} = 0$$
$$T > 3.23\,K$$
$$c_{UC} = -2.97\,x10^{-2}\,T + 9.62$$
$$T \leq 323\,K \qquad (26)$$
$$c_{UC} = 0$$
$$T > 3.23\,K$$

Figure 12 shows the departure function at 30°C. Note that the C18:2 data point was off the trend at all temperatures. There are very few data points and the outlier may arise from experimental error; more data is required to reach a conclusion. This data point was neglected when fitting Equation 23. The fit to the training data set is shown in Figure 11 (right). To test Equations 23 to 26, the vapour pressure of C16:1 is predicted, Figure 13. The correlation predicts the vapour pressure with an AARD of 2.4%.
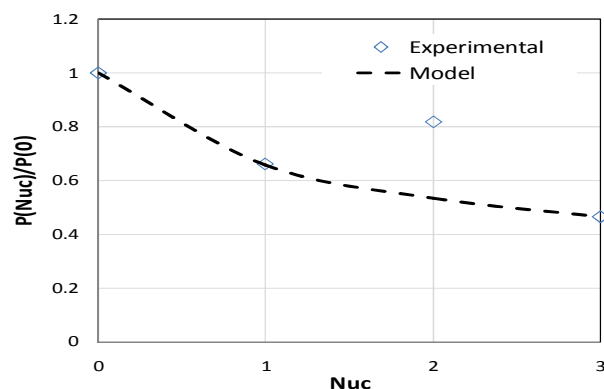

Fig. 12 Departure function for unsaturated C18 family of FAMEs at 30 °C
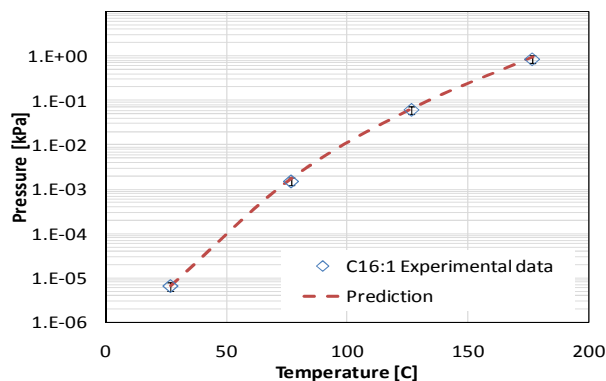

Fig. 13 Experimental and predicted values for methyl palmitoleate

V. BIODIESEL FUEL VAPOR PRESSURE

The vapour pressure of the biodiesel fuels listed in Table I was modeled using Raoult's law (Equation1). Figure 14 shows experimental and predicted vapour pressure data for canola and coconut biodiesel fuels. Two different scenarios were considered, the "All data" and "Constrained" scenarios, depending on which Cox parameters were used for the FAMEs (Table IV). In both cases, Raoult's Law fits the data well. AARD values are listed in Table V.

TABLE IV
COX EQUATION PARAMETERS FOR ALL-DATA AND CONSTRAINED-DATA SCENARIOS FOR FAMES

Formula	Scenario 1: All-Data				Scenario 2: Constrained-Data			
	$a_{PV,1}$	$a_{PV,2}[x10^3]$	$a_{PV,3}[x10^6]$	Pref [$x10^6$]	$a_{PV,1}$	$a_{PV,2}[x10^3]$	$a_{PV,3}[x10^6]$	Pref [$x10^6$]
C6:0	3.672	-1.151	1.058	25.833	3.534	-0.642	0.503	3.627
C8:0	2.973	1.854	-2.574	190.05	3.553	-0.694	0.481	108.04
C10:0	3.763	-1.330	1.074	75.905	3.603	-0.707	0.458	84.67
C12:0	5.053	-6.646	6.907	36.558	3.665	-0.776	0.494	69.242
C14:0	4.892	-5.432	5.252	19.399	3.752	-0.914	0.605	35.733
C15:0	3.970	-1.507	1.123	10.787	3.772	-0.758	0.389	12.351
C16:0	4.496	-3.269	2.685	8.846	3.791	-0.796	0.443	14.552
C17:0	4.121	-1.841	1.388	5.095	3.840	-0.883	0.541	6.454
C18:0	4.612	-3.409	2.740	3.297	3.854	-0.792	0.412	5.637
C20:0	3.987	0.102	-1.532	1.107	3.902	-0.866	0.501	3.021
C22:0	4.094	-0.659	-0.412	0.909	4.059	-1.245	0.716	1.695
C16:1**	3.952	0.0834	-0.703	0.000283	4.073	-0.784	0.520	0.000488
C17:1*	3.921	0.0570	-1.384	0.000129	4.110	-0.669	0.350	0.000216
C18:1(9)**	4.242	-0.851	0.255	0.000145	4.288	-1.080	0.527	0.000149
C20:1(11)*	4.397	-1.459	1.070	0.000104	4.153	-0.679	0.381	0.000219
C22:1**	4.457	-1.541	0.995	0.000193	4.299	-1.087	0.647	0.000324
C18:2**	3.982	0.656	-1.324	0.001550[a]	4.233	-0.855	0.600	0.004187[a]
C18:3**	2.552	6.982	-8.629	0.003519[a]	4.280	-0.810	0.560	0.000447[a]

a. Reference pressure Pref multiplied by 10^9

TABLE V
AVERAGE ABSOLUTE RELATIVE DEVIATION (AATD) PERCENTAGE FOR BIODIESEL FUEL VAPOR PRESSURE AND LIQUID HEAT CAPACITY PREDICTION

FAMEs	Code	All Data		Constrained	
		P_V	C_{PL}	P_V	C_{PL}
Canola (South Alberta)	CB-01	5.79	7.26	4.14	2.38
Canola (Saskatchewan)	I-25		3.61		4.20
Soy (Sunrise, US)	SB100		7.61		1.40
Soy (Mountain Gold, US)	MGB100	5.91	4.51	9.04	0.25
Rapeseed (Europe)	S102550	1.53	11.17	1.23	1.26
Palm (Europe)	S090824	3.11	19.73	1.60	2.49
Coconut (Europe)	S070717	12.73	40.95	9.45	0.42
Tallow (Alberta)	I26		7.67		0.68
Tallow (South Alberta)	Sylfat		12.61		4.57
Soybean (Idaho)		12.30	-	15.57	-
Rapeseed (Idaho)		4.69	-	1.99	-
Beef Tallow (Idaho)		6.94	-	6.52	-
Total		**-**	**6.62**	**12.79**	**6.19**

TABLE VI
NOMENCLATURE

Symbol	Definition	Units
$a_{PV,i}$	Adjustable parameter for Equation 4	-
ΔC_P	Phase transition heat capacity	kJ/kmol·K
$C_{P,L}$	Liquid heat capacity	kJ/kmol.K
C_P^0	Ideal gas heat capacity	kJ/kmol.K
C_P^{Res}	Residual heat capacity	kJ/kmol.K
J	Optimization objective function	-
MW	Molecular mass	Kg/k-mol
N_{UC}	Number of unsaturated carbon	-
P, P^V	Pressure, Vapour pressure	kPa
T	Temperature	K
T_{Ref}	Reference temperature	-
x_i	Mole fraction	-
α	Similarity function, Equation 12	-
ν	Stoichiometric value of an element in a compound	

Fig. 15 Experimental and predicted liquid heat capacity of canola and coconut biodiesel fuels; predictions made with analytical approach

VI. CONCLUSIONS

The vapour pressure of fatty acid methyl esters was modeled using the Cox equation. It was shown that an unconstrained correlation of the vapour pressure may lead to severe deviations in the predicted liquid heat capacity. The constrained correlations acceptably fit both the vapour pressure and liquid heat capacity data. The constrained equation is expected to provide less uncertain predictions of vapour pressure at pressure values close to or below 10^{-4} kPa where reliable vapour pressure experimental data may not be available. New correlations for vapour pressure, liquid heat capacity, and ideal gas heat capacity for FAMEs were also proposed. The vapour pressure and heat capacity of different biodiesel fuels was modeled assuming an ideal solution of FAMEs with an AARD of 6.2 and 2.0%, respectively.
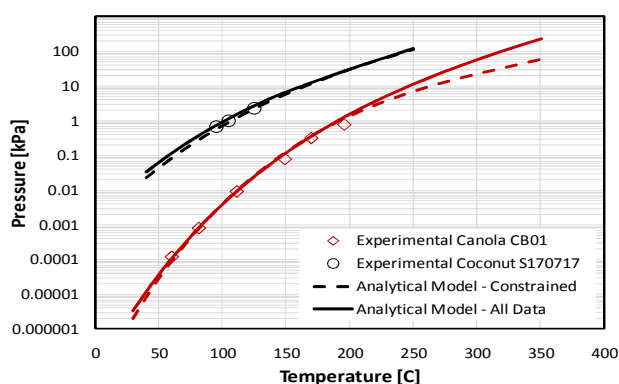
Fig. 14 Experimental and predicted vapour pressure of canola and coconut biodiesel fuel; predictions made with analytical approach (Data from Goodrum [2])

Biodiesel fuel heat capacities were also evaluated, Table V. Since only liquid heat capacity data were available, the predicted liquid heat capacities were calculated for the purpose of comparison as follows:

$$C_{P,L,Biodiesels} = \Delta C_{P,Biodiesels}^{Exp} + \sum_i C_{P,i}^0 , \qquad (27)$$

where *i* stands for the FAMEs that comprised the biodiesel fuels. Figure 15 compares the experimental and predicted (Equation27) liquid heat capacities. The "Constrained" scenario provided more accurate predictions of the heat capacities than the "All data" scenario (Table V). Also, the heat capacity may have an incorrect tendency to decrease with temperature; this behaviour was found to be significant when lighter FAMEs comprise the biodiesel fuels, Table II. Note that the liquid heat capacity was not predicted with the same accuracy as the FAMEs (2% versus 0.7%, Figures 6 and 7). The poorer prediction may result from slightly non-ideal behaviour in the biodiesel fuel liquid phase.
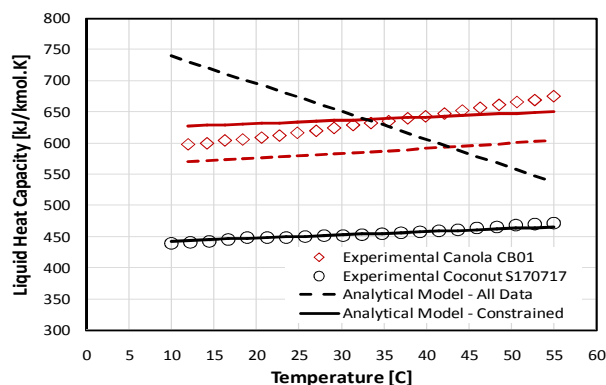
REFERENCES

[1] Allen, C. A. W.; Watts, K. C.; Ackman, R. G.; and Peg, M. J. Predicting the Viscosity of Biodiesel Fuels from Their Fatty Acid Ester Composition*, Fuel*, 78, 1999, 1319-1326.
[2] Goodrum, J. W. Volatility and Boiling Points of Biodiesel from vegetable Oils and Tallow, *Biomass and Bioenergy*, 22, 2002, 205-211
[3] Ott, L.; and Bruno, T. Variability of Biodiesel Fuel and Comparison to Petroleum-Derived Diesel Fuel: Application of a Composition and Enthalpy Explicit Distillation Curve Method, *Energy & Fuel*, 22, 2008,2861-2868
[4] Conceiçao, M. M., Roberlúcia, A. C., Silva, F. C., Bezerra, A. F., Fernandes Jr., V. J., and Souza, A. G. Thermoanalytical Characterization of Castor Oil Biodiesel, *Renewable & Sustainable Energy Reviews*, 11, 2007, 964-975
[5] Yuan, W., Hansen, A. C.; Zhang, Q. Vapor Pressure and Normal Boiling Point Predictions for Pure Methyl Esters and Biodiesel Fuels, *Fuel*, 84, 2005,943-950
[6] National Institute of Standards and Technology, NIST, NIST/EPA/NIH Mass Spectral Library Version 1.0, USA, 1995
[7] American Oil Chemist's Society (AOCS), The Lipid Library, USA, 2001

[8]   Bruno, T. J., and Svoronos, P. D. N., CRC Handbook of Fundamental Spectroscopic Correlation Charts, Taylor and Francis Group, 2006

[9]   Bruno, T. J., and Svoronos, P. D. N., CRC Handbook of Basic Tables for Chemical Analysis, Third Edition, CRC Press, Boca Raton, 2011

[10] Haines, P. J., Thermal Methods of Analysis: Principles, Applications and Problems, Springer, 2002

[11] Weir, R. D., and de Loos, Th. W. Measurement of the Thermodynamic Properties of Multiple Phases, IUPAC, Physical Chemistry Division, Commission on Thermodynamics, Elsevier, The Netherlands, 2005

[12] Knothe, G.; van Gerpen, J., and Krahl, J., The Biodiesel Handbook, AOCS Press, 2005

[13] Rúžička, K; and Majer, V. Simple and Controlled Extrapolation of Vapor Pressures toward the Triple Point, *AIChE J.*, 42 (6), 1723-1740, 1996

[14] National Institute of Standards and Technology, NIST. ThermoData Engine (TDE) Version 6.0, Pure compounds, Equations of state, Binary mixtures, and Chemical Reactions. NIST Standard reference Database #103b. Thermophysical Research Center. USA. 2011

[15] Roth, A. Vacuum Technology, 3rd edition, North-Holland, Netherlands, 1990

[16] Fulem, M., Private Communication, University of Calgary, Calgary, 2011

[17] Poling, B. E., Prausnitz, J. M., and O'Connell, J. P., The Properties of Gases and Liquids, 5th edition, McGraw-Hill, 2001

[18] Dadgostar, N.; and Shaw, J. A Predictive Correlation for the Constant-Pressure Specific Heat Capacity of Pure and Ill-Defined Liquid Hydrocarbons, *Fluid Phase Equilibria*, Paper in Press, 2011